CARBON 50 (2012) 347–355

Available at www.sciencedirect.com

SciVerse ScienceDirect

journal homepage: www.elsevier.com/locate/carbon

Mechanical characterization of aligned multi-walled carbon nanotube films using microfabricated resonators

Yoonjin Won [a,*], Yuan Gao [a], Matthew A. Panzer [a], Senyo Dogbe [b], Lawrence Pan [c], Thomas W. Kenny [a], Kenneth E. Goodson [a]

[a] Department of Mechanical Engineering, 440 Escondido Mall, Stanford University, Stanford, CA 94305, USA
[b] Stanford Nanofabrication Facility, Paul G. Allen Building, 420 Via Palou Mall, Stanford University, Stanford, CA 94305, USA
[c] Molecular Nanosystems Inc., 977 Commercial Street, Palo Alto, CA 94303, USA

ARTICLE INFO

Article history:
Received 17 March 2011
Accepted 8 August 2011
Available online 16 August 2011

ABSTRACT

Owing to their unique mechanical and thermal properties, vertically aligned carbon nanotube (VACNT) films are promising for use as advanced thermal interface materials. While there has been much research on the thermal properties of VACNT films, the mechanical modulus along the in-plane direction has received little attention. This paper reports a new technique for measuring this property using the resonant frequency shift in microfabricated resonators integrated with VACNT films. A comprehensive description of the technique includes microfabrication details, the laser Doppler methodology for extracting the resonant frequency, uncertainty analysis, and a model for data interpretation. A model accounting for the spatial variation of nanotube alignment relies on electron microscopy data and is consistent with the strong thickness dependence of the modulus data. The modulus of 0.5–100 μm-thick multi-walled nanotube films varies from 8 to 300 MPa, which is a promising value for a variety of applications including thermal interfaces.

1. Introduction

The high tensile strength, flexibility, and thermal conductivity of carbon nanotubes (CNTs) have motivated numerous studies on individual nanotubes, CNT composites, bundles, and films. There has been much recent interest in nanostructured thermal interface materials (TIM) composed of vertically aligned carbon nanotubes (VACNTs). While individual nanotubes are known to have high stiffness, VACNT film characterization has yielded a comparatively low axial elastic modulus due to the flexibility and large aspect ratio of individual tubes [1,2]. The geometry of VACNTs maximizes the desired low thermal resistance and mechanical compliance of a TIM [3–6].

The majority of mechanical characterization studies extracted the vertical elastic modulus of VACNT films using a nanoindentation technique to compress the film in the out-of-plane direction. McCarter et al. [7] found that the mechanical stiffness ranges from 30 to 80 MPa for a sample with fewer tube–tube contact sites to 100–300 MPa for a sample with a greater number of contacts. Other nanoindentation studies consistently yield elastic modulus values in similar ranges [8–13]. Unlike the extensive data available for the out-of-plane direction, the data for the in-plane modulus of VACNT films are limited even though this modulus is a critical property for TIM applications. Olofsson et al. [14] used a parallel plate capacitor fabricated using the techniques of microelectromechanical systems to determine the effective modulus of vertically aligned VACNT walls under lateral bending, measuring values between 1 and 10 MPa. Deck et al. [13] applied compression tests both in-plane and out-of-plane and found that the tubes are nearly five times stiffer in the out-of-plane direction. While several authors have observed

* *Corresponding author:* Fax: +1 650 7237657.
E-mail address: yoonjin@stanford.edu (Y. Won).
0008-6223/$ - see front matter
doi:10.1016/j.carbon.2011.08.009

the dependence of mechanical behavior on the microstructure of CNT films [7,10], models that quantify tube structures to predict their elastic behaviors are lacking. Some models of CNT-polymer composites include the dependence of elastic modulus on volume fraction, density, and diameter distribution [15]. Berhan et al. extensively analyzed randomly oriented nanotube sheets but have not translated the analysis to VACNT films [16,17].

We develop a measurement technique to extract the in-plane mechanical modulus of nanostructured films using the microfabricated resonator shown in Fig. 1. Using a laser Doppler vibrometer (LDV) system, we measure the resonant frequency of a cantilever beam with and without a multi-walled carbon nanotube (MWCNT) film grown on top. The shift in resonant frequency of the beam due to the presence of the MWCNT film provides a means to calculate the modulus using beam theory. Beam dimensions are scaled to achieve a range of estimated resonant frequencies. Varying the thicknesses of the MWCNT films illustrates the effect of film thickness on their mechanical properties. The results are compared with predictions of the modulus based on the film morphology.

2. Sample design and fabrication

2.1. Fabrication process

The resonator fabrication begins with a single-crystal, double-side polished Si substrate, as shown in Fig. 2. A 0.5 μm-thick SiO_2 film is grown in a furnace with a constant temperature of 1000 °C. The epitaxial polysilicon films with varying thicknesses are deposited on the substrate. The substrate is subjected to a deep reactive ion etching (DRIE) with a mask of the cantilever outlines from the front side. Another DRIE with a mask of the cantilevers from the backside opens the bottom substrate, using the thermally grown SiO_2 layer as an etch-stop layer. After completing the DRIE steps, the SiO_2 layer is removed using a plasma etching, which displays a high selectivity for SiO_2. The cantilever dimensions are shown in Table 1.

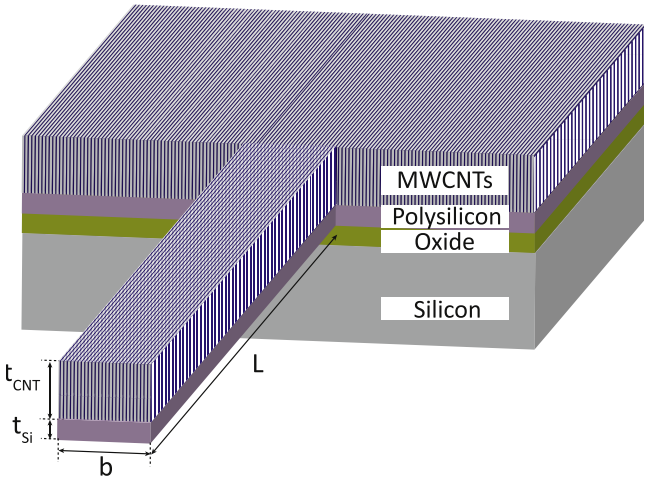

Fig. 1 – Schematic of a polysilicon and MWCNT composite beam. Beam dimensions are varied to achieve a range of resonant frequencies. The film thicknesses of the MWCNT are varied to measure the thickness dependence.

2.2. Growth procedure of MWCNT films

The growth procedure for vertically aligned MWCNT films starts with the deposition of a 200 Å Al_2O_3 film and a 10 Å Fe catalyst film on the front side of the patterned substrate. Substrates are cleaved to 1 cm × 1 cm samples, each containing roughly 80 cantilevers. The MWCNT films are grown on the substrates using chemical vapor deposition (CVD). The growth process involves heating the substrates to high temperatures in a reactor. Annealing in H_2 produces a monolayer of Fe clusters that act as catalysts for the MWCNT growth. A mixture of C_2H_4, H_2 and Ar gases flows through the chamber at 800 °C to produce a dense array of MWCNTs. Carbon nanotubes grow from the particles via the catalytic dissociation of hydrocarbon molecules by the metal particles and the dissolution of carbon atoms into the particle. Upon saturation, carbon atoms precipitate from the metal particles in a way that favors the formation of tubular carbon structures. Dense arrays of 0.5–100 μm-thick aligned nanotubes are attained by varying the growth duration over three growth runs. Fig. 3 provides scanning and transmission electron microscope images of the MWCNTs on a resonator. The scanning electron microscope images in Fig. 3a and b shows dense film of vertically aligned MWCNTs grown on a resonator. This image suggests that a MWCNT film can be approximated as a continuum, which can be applied to the composite beam analysis. The transmission electron microscope image in Fig. 3c shows that each multi-walled nanotube is comprised of roughly 25–30 walls with inner diameter of 10 nm and outer diameter of 30 nm.

3. Measurement methodologies

3.1. Measurement procedure

A LDV characterizes the mechanical properties of MWCNT films by measuring the resonant frequency of the cantilevers. One major advantage of using the LDV together with the microresonator sample is the simplicity in the fabrication process [18,19]. Other techniques, including capacitive and piezoresistive detection, require more steps in the fabrication process, such as conductive implantations, which may complicate nanotube growth. In addition to the measurement of mechanical characteristics using the LDV, a thermoreflectance measurement used previously on CNT films can be performed on a separate region of the sample [3,5], as indicated in Fig. 4a. Our mechanical characterization structure enables the optical characterization of both the mechanical and thermal properties of identical nanotube arrays of samples in close proximity, which is the focus of future research. Fig. 4b shows a scanning electron microscope image of the resonators after the fabrication process.

For the LDV procedure, the cantilevers are mounted on a piezoelectric shaker inside a vacuum chamber with optical access. The shaker is driven by a 150 mV white noise input with frequency ranging from 1 kHz to 350 kHz and amplified

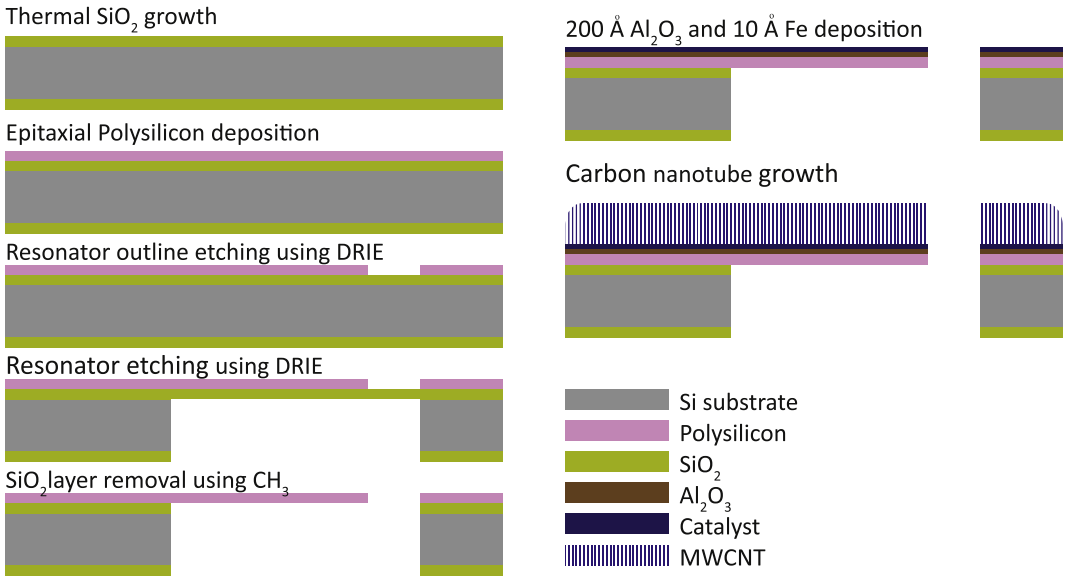

Fig. 2 – Microresonator fabrication process and MWCNT film growth. Using this process, we can vary the SiO_2 and polysilicon thicknesses. The SiO_2 growth step can be substituted with commercial silicon on insulator substrates in the future. After the process, a completed wafer contains more than 3000 cantilevers.

Table 1 – Beam parameters and dimensions.

Material	Parameter	Dimension
Polysilicon	L	200–3000 μm
	b	25–100 μm
	t_{Si}	6.8–8.7 μm
	ρ_{Si}	2330 kg/m^3
MWCNT	t_{CNT}	0.4–110 μm
	ρ_{CNT}	29–56 kg/m^3

at fixed 100 × gain by a Krohn-Hite 7500 Wideband Power Amplifier. The beam from a Polytec OFV 2500 LDV is directed at the end of the cantilever, and the frequency of the scattered light is extracted from the Doppler shift f_D. The Doppler shift is a function of the velocity component in the direction of the object beam, v_{beam}, according to $f_D = 2 \cdot v_{beam}/\lambda$, where λ is the laser wavelength. The output is filtered through a velocity filter and recorded to a vector signal analyzer (HP89441A) to find the peaks of the vibration. The vector signal analyzer, which is connected to a personal computer (PC) via general purpose interface bus (GPIB) (NI-GPIB-USB-HS, National Instruments), controls the operating frequency range of the shaker as well. To increase the signal magnitude, we maintain the perpendicular alignment of the laser at the end of the beam. Fig. 5 shows an image and a simplified control diagram of the LDV setup. The resonant frequency of each microfabricated cantilever is measured before and after the growth of MWCNT films.

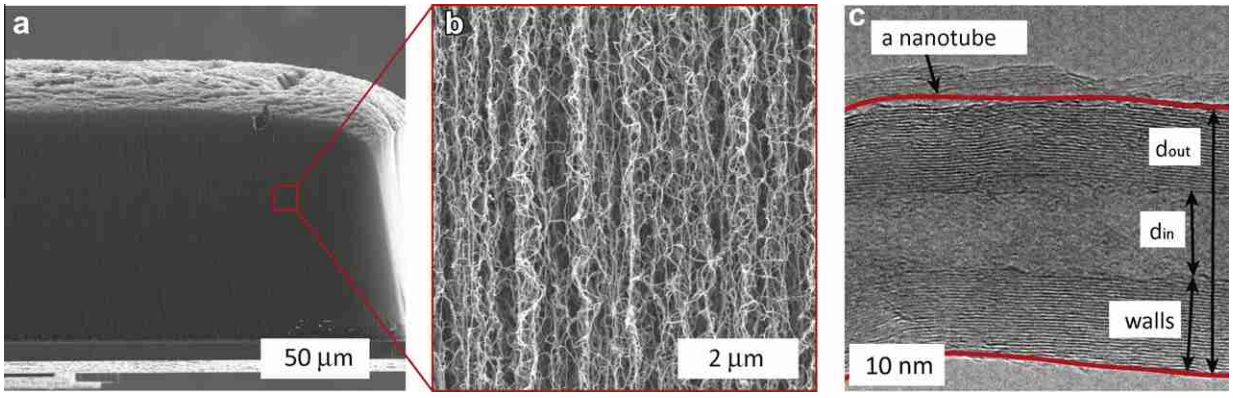

Fig. 3 – (a) Scanning electron microscope (SEM) image of a 100 μm-thick MWCNT film on a microresonator. (b) SEM image showing that the detailed morphology of a MWCNT film has a high degree of entanglement between the nanotubes. (c) Transmission electron microscope image of a single MWCNT taken from the film samples studied in this manuscript. The outer diameter of the nanotube is approximately 30 nm, the inner diameter is approximately 10 nm, and there are 25–30 walls.

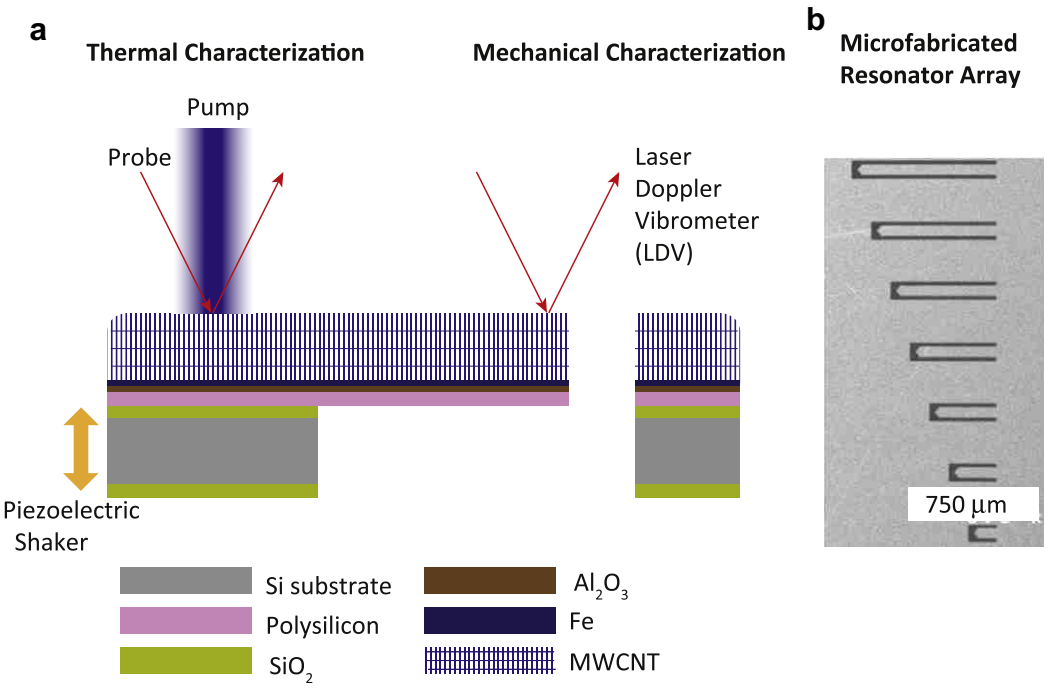

Fig. 4 – (a) Schematic of the mechanical characterization structure. The structure allows simultaneous measurement of the thermal and mechanical properties using optical techniques. (b) SEM image of resonator arrays after the fabrication process, showing the variation in cantilever length to obtain various resonant frequencies.

3.2. *Data interpretation and analysis*

The mechanical properties of the CNT films are extracted by comparing the LDV frequency response data to the frequency response calculated from a model of the silicon cantilever and CNT film as a two-layer composite beam by using beam theory. The assumptions in the linear beam bending theory include slender beams, a constant cross-section, small deflections and linear elastic behavior during bending.

3.2.1. *Resonant frequency of a composite beam*

Solving the one-dimensional Euler–Bernoulli differential equation (1) for a fixed-free beam yields the resonant frequencies of the cantilever:

$$\rho A\frac{\partial^2 v}{\partial t^2}+EI\frac{\partial^4 v}{\partial x^4}=0 \tag{1}$$

Here $v(x,t)$ is the time dependent transverse displacement of the cantilever beam, EI is the bending stiffness, ρ is the density, and A is the cantilever cross-sectional area. The displacement, $v(x,t)$ can be solved using separation of variables into the time and spatial components (2):

$$v(x,t)=V(x)\cdot Y(t) \tag{2}$$

For the undamped cantilever beam, the resonant frequency corresponding to the nth mode is

$$w_n-2\pi f_n=\lambda_n^2\sqrt{\frac{EI}{\rho A}}=\frac{z_n^2}{L^2}\sqrt{\frac{EI}{\rho A}} \tag{3}$$

where $z_1=\lambda_1 L=1.875$, $z_2=\lambda_2 L=4.694$, and $z_3=\lambda_3 L=7.855$.

The Euler–Bernoulli differential equation solutions provide the resonant frequency of a composite beam with uniform cross-sectional by replacing EI and ρA with the appropriately modified bending stiffness $\overline{EI}$ and linear mass density $\overline{\rho A}$ [20,21]. The resonant frequency of a composite beam with N layers is then given by

$$w_n=2\pi f_n=\lambda_n^2\sqrt{\frac{\overline{EI}}{\overline{\rho A}}}=\frac{z_n^2}{L^2}\sqrt{\frac{\overline{EI}}{\overline{\rho A}}} \tag{4}$$

where

$$\overline{EI}=\sum_{i=1}^{N}E_iI_i,\quad \overline{\rho A}=\sum_{i=1}^{N}\rho_iA_i \tag{5}$$

In Eq. (5), ρ_i is the density and A_i, E_i and I_i are the cross-sectional area, elastic modulus, and moment of inertia of each individual layer, respectively. The resonant frequency shift between a silicon beam and a Si-CNT beam is

$$\Delta w_n=\frac{z_n^2}{L^2}\left(\sqrt{\frac{E_{Si}I_{Si}+E_{CNT}I_{CNT}}{\rho_{Si}A_{Si}+\rho_{CNT}A_{CNT}}}-\sqrt{\frac{E_{Si}I_{Si,0}}{\rho_{Si}A_{Si}}}\right) \tag{6}$$

To calculate I_{Si} and I_{CNT}, we use the transformed section method. The cross-section of a composite beam is transformed into an equivalent cross-section of an imaginary beam composed of same material where b_i, the width of each normalized layer, is given by Eq. (7),

$$b_i=\frac{E_i}{E_N}b_N \tag{7}$$

where b_N is the width of the top layer, E_i is the Young's modulus of each layer, and E_N is the Young's modulus of the top layer. Thus, I_{Si}, I_{CNT} and the location of the neutral plane relative to the bottom of the beam, y, are computed by the following equations:

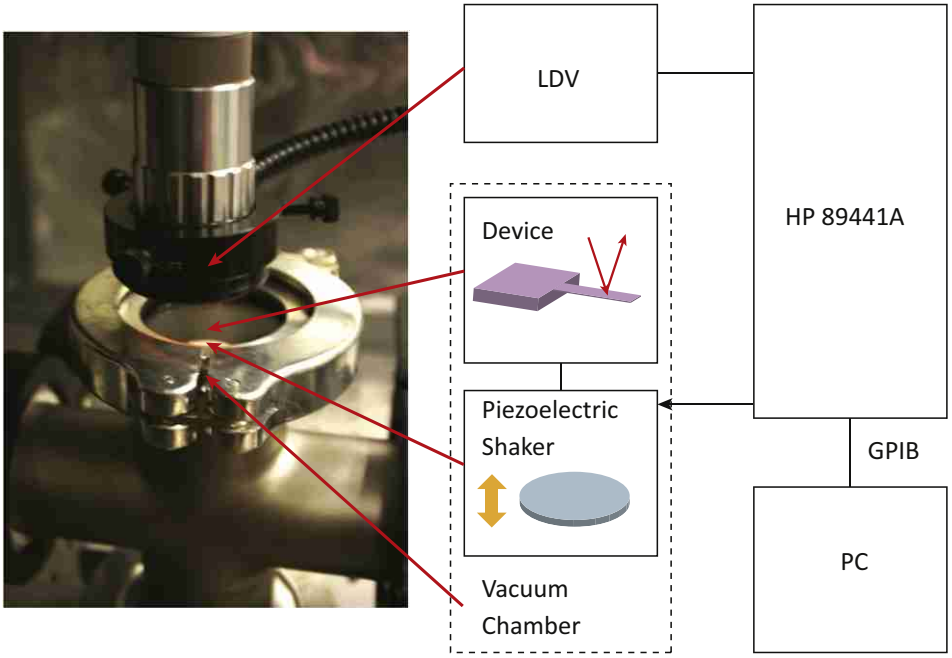

Fig. 5 – Image and control diagram of the LDV system. A signal generator excites a piezoelectric disk around the cantilever's fundamental resonant frequency. The resulting frequency spectrum from the LDV is recorded.

$$y = \frac{\sum_{i=1}^{N} d_i A_i}{\sum_{i=1}^{N} A_i} = \frac{\frac{1}{2} t_{Si} \cdot \frac{E_{Si}}{E_{CNT}} b t_{Si} + \left(t_{Si} + \frac{t_{CNT}}{2}\right) \cdot b t_{CNT}}{\frac{E_{Si}}{E_{CNT}} b t_{Si} + b t_{CNT}}$$
$$= \frac{E_{Si} t_{Si}^2 + E_{CNT}(2t_{Si} + t_{CNT}) t_{CNT}}{2E_{Si} t_{Si} + 2E_{CNT} t_{CNT}} \quad (8)$$

where

$$I_{Si} = \frac{b t_{Si}^3}{12} + A_{Si}\left(y - \frac{t_{Si}}{2}\right)^2 \quad (9)$$

$$I_{CNT} = \frac{b t_{CNT}^3}{12} + A_{CNT}\left(t_{Si} + \frac{t_{CNT}}{2} - y\right)^2 \quad (10)$$

3.2.2. *Elastic modulus of a composite beam*

The ratio of the resonant frequency shift of a beam with a CNT layer to the original resonant frequency of the bare silicon beam is given by the following equation:

$$\delta = \frac{\Delta w_n}{w_{n,Si,0}} = \sqrt{\frac{E_{Si} I_{Si} + E_{CNT} I_{CNT}}{\rho_{Si} A_{Si} + \rho_{CNT} A_{CNT}}} \cdot \sqrt{\frac{\rho_{Si} A_{Si}}{E_{Si} I_{Si,0}}} - 1 \quad (11)$$

The mass densities of the CNT films are determined using the measured mass of the CNT films, film thicknesses, and areas. The mass of the sample in its entirety before and after the nanotube growth is measured using a microbalance (SE2 Ultra Micro Balance, Sartorius). The density is confirmed by removing the CNT film and re-weighing the substrate. From the measured frequency shift, δ, and the material properties, solving Eq. (11) for the CNT modulus yields:

$$E_{CNT} = \frac{E_{Si}}{I_{CNT}}\left(\left(1 + \frac{\rho_{CNT} A_{CNT}}{\rho_{Si} A_{Si}}\right) \cdot (1+\delta)^2 I_{Si,0} - I_{Si}\right) \quad (12)$$

Although CNT film thickness is important in determining the modulus, it is difficult to achieve a uniform CNT film thickness across the microfabricated cantilevers because the resonator geometry influences the nanotube growth. The resulting nonuniformity of the film thickness complicates data interpretation. To estimate the impact of nonuniformity, we perform an analysis based on thickness variations $t_{CNT} = \overline{t_{CNT}} \pm e$, where e is the variation in thickness. The effective modulus with the nonuniformity is expressed as

$$E_{CNT,eff} = E_{Si}\left(\left(1 + \frac{\rho_{CNT}(\overline{t_{CNT}} + e) b}{\rho_{Si} A_{Si}}\right) \cdot (1+\delta)^2 I_{Si,0} - I_{Si}\right) \cdot \left(\frac{b}{12}\left(\overline{t_{CNT}^3} \pm 3\overline{t_{CNT}^2} e\right) + \frac{A_{CNT}}{2}(\alpha)^2 \pm A_{CNT}(\alpha) e\right)^{-1} \quad (13)$$

where

$$\alpha = 2t_{Si} - 2y + \overline{t_{CNT}} \quad (14)$$

and where each nanotube growth contains a different nonuniformity. These nonuniformities are used to calculate the error bars in Figs. 6 and 9. Here the beam equations assume that the length is 20 times the thickness, but several thicker films do not satisfy this assumption. To account for this, we calculate a correction factor using film modeling. We apply the modulus values from the measurement to the finite element model to obtain the frequency shifts from the model. Then the frequency shifts are entered as the input parameters into the two-layer analysis to recalculate the modulus. There is a slight difference of 0–2 MPa between the initial and recalculated moduli. The difference increases linearly with thicknesses with a coefficient of 0.00153 μm^{-1} MPa^{-1}, which is used as a correction factor for the moduli calculation using the Euler–Bernoulli analysis.

3.3. *Validation of measurement technique and uncertainty analysis*

We establish confidence in this new technique by measuring the modulus of an e-beam evaporated, 0.9 μm-thick Al film on

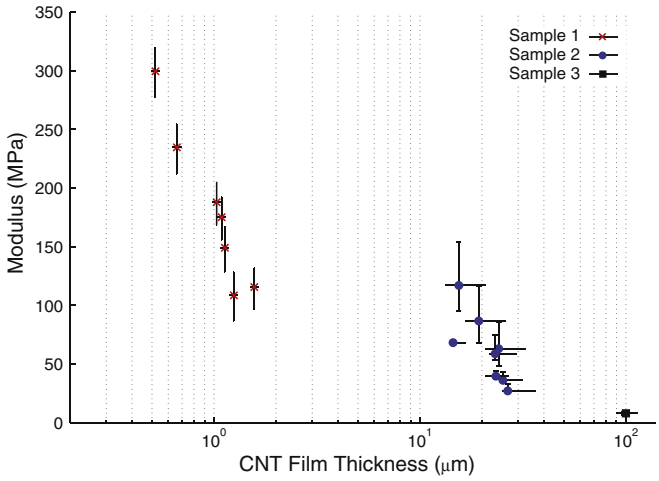

Fig. 6 – Effective modulus of MWCNT films from three separate growths: samples 1 and 2 include films of thickness 0.5–1.6 μm and 15–27 μm, respectively. Sample 3, which contains one cantilever, has a thickness of 100 μm. The film densities are 31–32 kg/m^3 (Sample 1), 55–56 kg/m^3 (Sample 2), and 29 kg/m^3 (Sample 3).

8.7 μm-thick polysilicon resonators. Using Eq. (11) and the properties of Al and polysilicon, we predict the frequency shift to be 1.8%. The measured frequency shift of 1.7–2.0% agrees with the calculation with −5.5% to 8.7% error. Using the measured frequency shift in Eq. (12) yields the modulus of Al to be 67.9–70.3 GPa, which agrees with the established modulus of 69 GPa for Al with −1.6% to 1.9% error and demonstrates the accuracy of this technique to extract the modulus of thin films. We also validate the analytical model of the poly-Al composite beam using a finite element analysis program (COMSOL 4.0). The predicted resonant frequency for Al on polysilicon beams with various lengths (500–1000 μm) agrees with the measurements with errors of −0.6% to 5.6%.

The sources of uncertainty in this technique include equipment resolution as well as nonuniformity of film thickness. Since the vector signal analyzer collects data for a finite record length using a fixed value of 1601 points, narrower frequency spans have finer resolution. The measurements are conducted at frequency spans of 2, 5, 10, and 20 kHz yielding frequency resolutions of 1.25, 3.125, 6.25, and 12.5 Hz. For each measurement, we ensure that the resolution is small enough to detect the minimum resonant frequency shift. The frequency shifts range from −0.03% to −0.1% for sample 1, −0.4% to −1% for sample 2, and −5% for sample 3. These frequency shifts are used as the input parameters to calculate the effective modulus. The resonant shift is 80–100 Hz for the thin films and up to 8 kHz for the thick films. We perform additional measurements to account for the temporal effect and the laser alignment effect on the resonant frequencies. First, we measure the resonant frequencies over a one-month period, and they are quite stable with a 0.008–0.05% shift. We also measure resonant frequencies at several different points along a long resonator, and the results yields identical frequencies regardless of the laser location.

4. Results and discussion

4.1. *Data interpretation and results*

The measured frequency shifts are input parameters to the two-layer analysis described in Section 3 to calculate the modulus of different MWCNT film thicknesses. Fig. 6 shows the extracted modulus of different nanotube film thicknesses

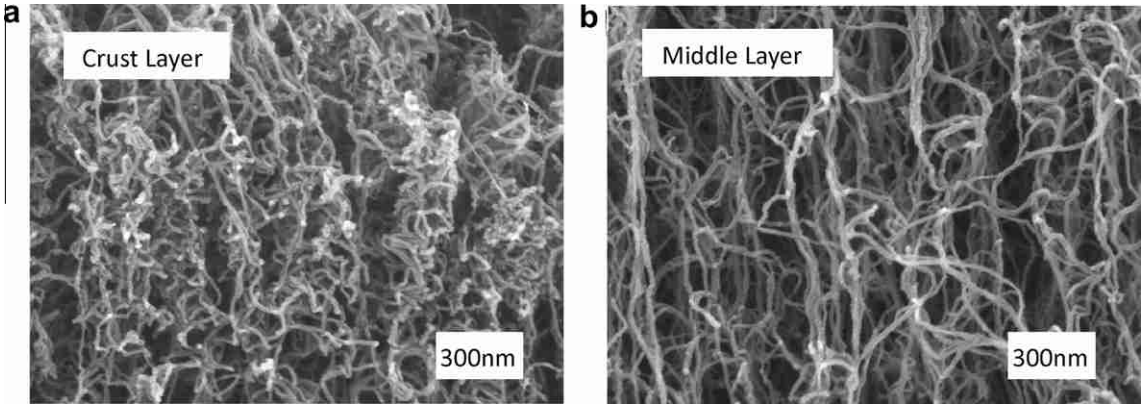

Fig. 7 – SEM images of the crust and middle layer in a MWCNT film. (a) The crust layer exhibits more entanglement than the rest of the film. (b) The middle layer has straighter MWCNTs with lower density.

resulting from three growths. The horizontal error bars represent the nonuniformity of MWCNT films. The vertical error bars represent the range of the resulting effective modulus of MWCNT films due to their thickness nonuniformities. Fig. 6 indicates that the calculated modulus ranges from 8 to 300 MPa for 0.5–100 μm-thick films. As Fig. 6 shows, thin films are more uniform in thickness on an absolute scale, with average thickness variations of 0.2 μm in sample 1. Because these variations are large relative to the film thickness, however, the variations in the extracted modulus are large. The cantilevers of sample 2 and sample 3 have thickness variations of 2–10 μm and 25 μm respectively. Though these variations are larger than the variations in the thin films, the effect on the modulus is smaller. The impact of the thickness nonuniformity on the modulus of thin films is thus stronger than that of thick films.

4.2. *Effective modulus of nonhomogeneous MWCNT films*

Nanotube characteristics such as alignment, density, and radius will all affect the mechanical behavior of the nanotube films. Zhang et al. [22] observed the growth process of VACNT using SEM, resonant Raman spectroscopy, and angle-resolved X-ray absorption. These measurements revealed two different stages during the growth process. The first step is the interweaving of a thin layer of entangled and randomly-oriented nanotubes, forming a crust. The second step is the vertically aligned growth beneath the top crust. Fig. 7 displays a similar morphology for our films displaying a thin, entangled crust layer above a more vertically oriented layer. Fig. 8 schematically illustrates this thickness-dependent structure of MWCNT films. Since the nanotubes are more entangled and dense in the crust, the crust layer is potentially stiffer than the middle layer. During beam bending, the maximum stresses occur at the top and bottom surfaces, so the mechanical properties of the crust will have a strong influence on the mechanical stiffness response during measurement. Therefore, a film thickness dependence of the MWCNT modulus due to the presence of the crust layer is expected. To illustrate the relation between the effective modulus and the MWCNT film thickness, we introduce a three-layer analysis comprised of the crust, middle, and substrate layer in Section 4.3.

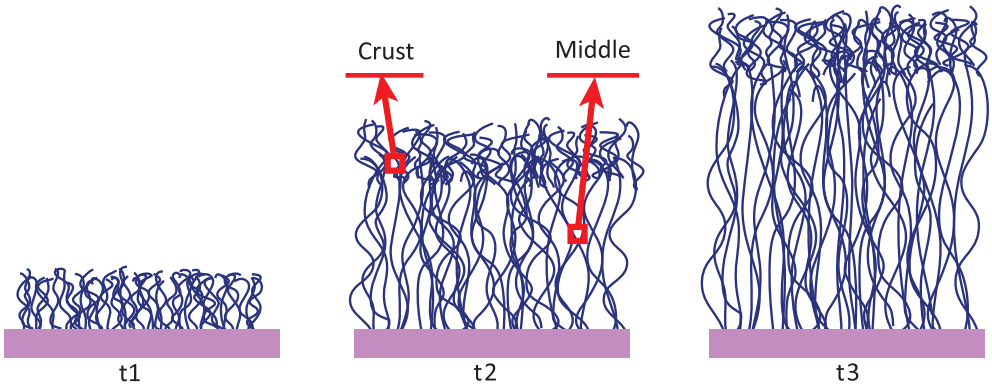

Fig. 8 – Schematics of the thickness-dependent structure of MWCNT films, with growth time increasing from t1 to t3. The structure at t1 represents the formation of the crust layer with 400 nm. As the growth progresses (t2), a more aligned middle section is formed below the crust, which continues to grow from the base (t3).

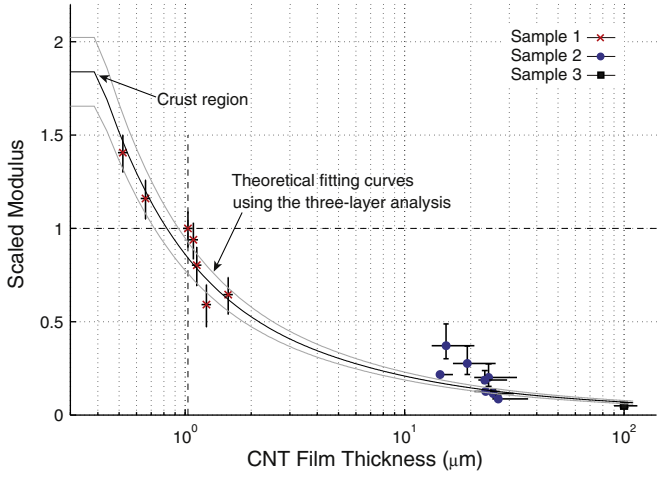

Fig. 9 – Theoretical fitting curves plotted against the scaled modulus to illustrate the thickness dependence of the elastic modulus of MWCNT films. The modulus is scaled here to reduce the effects of film density. The theoretical curves are calculated using the three-layer analysis over increasing middle layer thickness. The effective modulus significantly decreases with MWCNT film thickness as the relative impact of the high-modulus crust layer diminishes.

4.3. Total film behavior prediction based on crust and middle layer

Fig. 9 provides the scaled data and prediction of the modulus of the films in this study. Since it is very difficult to reproduce identical conditions between consecutive growth runs, each of the samples from the different runs exhibits a different morphology and density. Variations in the density exert a particularly strong influence on $E_{CNT,eff}$, as expressed in Eq. (13). For efficient representation of the modulus data, we scale $E_{CNT,eff}$ by the effective modulus of a reference sample, which has a 1 μm thickness. In addition, we reduce the density effect on the effective modulus by using a volume factor f_{volume} such that the films with different densities fall on one theoretical curve. The scaled modulus, $E^*_{CNT,eff}$ is given by

$$E^*_{CNT,eff} = \frac{E_{CNT,eff}}{E_{reference-CNT,eff}} \cdot \frac{1}{f_{volume}} \quad (15)$$

where f_{volume} is $\frac{\rho_{CNT}}{\rho_{reference-CNT}}$. The decrease in the extracted modulus with increasing MWCNT film thickness may result from the stiff crust layer, whose impact on the effective modulus diminishes for thicker films. Here we develop an approximate, qualitative model describing this trend based on the experimental data and an extension of the analytical technique presented in Section 3. To account for the different regions in a MWCNT film, we use a three-layer beam analysis in which the top layer is the crust, the middle layer is the aligned MWCNT section, and the bottom layer is the substrate. The resonant frequency shift of the three-layer beam is found using Eqs. (5) and (11) in Section 3.2 with $i = 3$. The calculated shift is re-applied as an input to calculate the effective modulus of a MWCNT film. This analysis uses the modulus from the thinnest MWCNT film as that of the crust layer. We determine that the thickness of the crust layer is about 400 nm using SEM images. Since SEM micrographs of crust and middle layer display different morphology and density, the difference in their densities need to be quantified. We use SEM images displaying both crust and middle layer in one image to maintain constant brightness and contrast. By comparing the average intensity in the crust and middle region, we estimate that the crust layer has approximately 40% greater density. Since each difference in densities is determined by each growth run, it would be interesting to see the dependency of growth conditions on the densities of the crust and middle layer. Therefore, the fitting parameters of densities eventually need to be investigated by identifying the growth process as well as using better quality of SEM images. By assuming that the middle layer modulus is not thickness dependent, we use the measured modulus and density of the 100 μm-thick film as the properties of the middle layer. The values shown in Table 2 are used in the three-layer analysis to obtain the theoretical curves in Fig. 9, which reflect the effect of increasing the middle layer's thickness. By varying the input modulus by ±10%, we illustrate the impact of these changes on the effective modulus of the MWCNT film.

This work leaves a number of questions open for future research. For example, the residual stresses in the wafer and resonator sample may influence the measured modulus. The deformation mechanism in a MWCNT film may be dissimilar from that of a solid structure, as the tubes are only held together by relatively weak van der Waals forces at the tube–tube contacts [23]. Another complication could include the presence of viscoelastic effects. There may be an instantaneous sliding of some tube–tube contacts under applied stress. Several authors have observed the time-dependent rearrangement in MWCNT films during beam bending [7,10,13,24]. However, the current lack of quantitative studies on these tube–tube friction forces makes it difficult to model how much tube–tube sliding contributes to the mechanical responses during the measurement. Therefore, future work will involve developing a model to account for tube–tube interactions and their viscoelastic effects. The qualify factor of the resonators will also provide insight into the viscoelastic behavior of the films.

Table 2 – Parameters used in the three-layer model. The range of values for $MWCNT_{middle}$ represents the range of thicknesses plotted.

	Thickness (μm)	Density (kg/m^3)	Modulus (MPa)
$MWCNT_{top}$	0.4	40.0	300 ± 30
$MWCNT_{middle}$	0–110	28.9	10 ± 1
Polysilicon	6.8–8.7	2330	$155 \cdot 10^3$

5. Summary and concluding remarks

We demonstrate here the first measurements of the in-plane modulus of aligned MWCNT films using microfabricated resonators and a LDV system. This technique will eventually allow measurement of both thermal and mechanical properties of MWCNTs under identical growth conditions. We provide an analysis for the thickness dependence of the modulus, which the data show to vary from 8 to 300 MPa for films in the thickness range of 0.5–100 μm. SEM micrographs indicate the presence of a crust layer of thickness ~400 nm, and a simple model accounting for a higher stiffness in this region is consistent with the data. The low elastic modulus of the MWCNT films indicates their mechanical suitability as an interface material, which typically has an elastic modulus of <2 GPa. This work provides motivational data for ongoing nanotube dynamics simulations by the authors, which account for the CNT film morphology and the intrinsic mechanical properties of the CNTs. The goal of these simulations is to illustrate the effects of these characteristics on the elastic modulus and to provide a more fundamental basis for predicting the mechanical response of CNT films. The next challenge is integration of the CNT TIM in real systems and observing how the film behaves under large strains imposed by the coefficient of thermal expansion mismatch of the bounding materials. Understanding the thermo mechanical properties of CNT films would greatly benefit from being performed in conjunction with thermal characterization of the CNT film.

Acknowledgements

This work was sponsored by the Office of Naval Research ONR (N00014-09-1-0296-P00004, Dr. Mark Spector, program manager), SRC, the MARCO IFC, and the National Science

Foundation. We would like to thank Molecular Nanosystems for their continued collaboration on MWCNT growth, specifically by providing the reaction chamber and technical guidance. We performed this work in part at the Stanford Nanofabrication Facility (a member of the National Nanotechnology Infrastructure Network), which is supported by the National Science Foundation under Grant ECS-Integrated Systems.

REFERENCES

[1] Yaglioglu O, Martens R, Hart A, Slocum A. Conductive carbon nanotube composite microprobes. Adv Mater 2008;20:357–62.
[2] Demczyk BG, Wang YM, Cumings J, Hetman M, Han W, Zettl A, et al. Direct mechanical measurement of the tensile strength and elastic modulus of multiwalled carbon nanotubes. Mater Sci Eng A 2002;334(1–2):173–8.
[3] Panzer MA, Zhang G, Mann D, Hu X, Pop E, Dai H, et al. Thermal properties of metal-coated vertically aligned single-wall nanotube arrays. J Heat Transfer 2008;130(5):052401.
[4] Tong T, Yang Z, Delzeit L, Kashani A, Meyyappan M, Majumdar A. Dense vertically aligned multiwalled carbon nanotube arrays as thermal interface materials. IEEE Trans Compon Pack Technol 2007;30(1):92–100.
[5] Gao Y, Marconnet A, Panzer M, LeBlanc S, Dogbe S, Ezzahri Y, et al. Nanostructured interfaces for thermoelectrics. J Elec Mater 2010;39(9):1456–62.
[6] Prasher R. Thermal interface materials: historical perspective, status, and future directions. Proc IEEE 2006;94(8):1571–86.
[7] McCarter CM, Richards RF, Mesarovic SD, Richards CD, Bahr DF, McClain D, et al. Mechanical compliance of photolithographically defined vertically aligned carbon nanotube turf. J Mater Sci 2006;41(23):7872–8.
[8] Cao A, Dickrell PL, Sawyer WG, Ghasemi-Nejhad MN, Ajayan PM. Super-compressible foamlike carbon nanotube films. Science 2005;310(5752):1307–10.
[9] Garcia E, Hart A, Wardle B, Slocum A. Fabrication nanocompression testing of aligned carbon-nanotube-polymer nanocomposites. Adv Mater 2007;19(16):2151–6.
[10] Mesarovic S, McCarter C, Bahr D, Radhakrishnan H, Richards R, Richards C, et al. Mechanical behavior of a carbon nanotube turf. Scripta Mater 2007;56(2):157–60.
[11] Zbib AA, Mesarovic SD, Lilleodden ET, McClain D, Jiao J, Bahr DF. Thecoordinatedbuckling of carbon nanotube turfs under uniform compression. Nanotechnology 2008;19(17):175704.
[12] Whitby RL, Mikhalovsky SV, Gun'ko VM. Mechanical performance of highly compressible multi-walled carbon nanotube columns with hyperboloid geometries. Carbon 2010;48(1):145–52.
[13] Deck CP, Flowers J, McKee GSB, Vecchio K. Mechanical behavior of ultralong multiwalled carbon nanotube mats. J Appl Phys 2007;101(2):023512.
[14] Olofsson N, Ek-Weis J, Eriksson A, Idda T, Campbell EEB. Determination of the effective young's modulus of vertically aligned carbon nanotube arrays: a simple nanotube-based varactor. Nanotechnology 2009;20(38):385710.
[15] Thostenson E, Chou TW. On the elastic properties of carbon nanotube-based composites: modeling and characterization. J Phys D Appl Phys 2003;36:573–82.
[16] Berhan L, Yi YB, Satsry AM. Effect of nanorope waviness on the effective moduli of nanotube sheets. J Appl Phys 2004;95:5027–34.
[17] Berhan L, Yi YB, Sastry AM, Munoz E, Selvidge M, Baughman R. Mechanical properties of nanotube sheets: alterations in joint morphology and achievable moduli in manufacturable materials. J Appl Phys 2004;95(8):4335–45.
[18] Barlian A, Park S, Mukundan V, Pruitt B. Design and characterization of microfabricated piezoresistive floating element-based shear stress sensors. Sens Actuators A 2007;134(1):77–87.
[19] Yasumura. Energy dissipation mechanisms in microcantilever oscillators with applications for the detection of small forces. Stanford, CA, USA, Stanford Univ, Ph.D thesis, 2004.
[20] Rast S, Wattinger C, Gysin U, Meyer E. Dynamics of damped cantilevers. Rev Sci Instrum 2000;71:2772–5.
[21] Voiculescu I, Zaghloul M, McGill R. Modelling and measurements of a composite microcantilever beam for chemical sensing applications. Proc Inst Mech Eng 2006;220:1601–8.
[22] Zhang L, Tan Y, Sakulchaicharoen N, Mun B. Influence of a top crust of entangled nanotubes on the structure of vertically aligned forests of single-walled carbon nanotubes. Chem Mater 2006;18(23):5624–9.
[23] Ajayan PM, Banhart F. Nanotubes: strong bundles. Nat Mater 2004;3(3):135–6.
[24] Zhang Q, Lu YC, Du F, Dai L, Baur J, Foster DC. Viscoelastic creep of vertically aligned carbon nanotubes. J Phys D Appl Phys 2010;43(31):315401.